

Dust Grain Growth at High Redshift: Starburst-driven CMB-Dark Supershells

Sergio Martínez-González ^{*1}, Sergiy Silich ², Guillermo Tenorio-Tagle²,

¹CONACYT-Instituto Nacional de Astrofísica, Óptica y Electrónica, AP 51, 72000 Puebla, México

²Instituto Nacional de Astrofísica Óptica y Electrónica, AP 51, 72000 Puebla, México

Accepted July 27th, 2021.

ABSTRACT

We present a novel scenario for the growth of dust grains in galaxies at high-redshift ($z \sim 6$). In our model, the mechanical feedback from massive star clusters evolving within high-density pre-enriched media allows to pile-up a large amount of matter into massive supershells. If the gas metallicity ($\geq Z_{\odot}$), number density ($\geq 10^6 \text{ cm}^{-3}$) and dust-to-gas mass ratio ($\sim 1/150 \times Z$) within the supershell are sufficiently large, such supershells may become optically thick to the starlight emerging from their host star clusters and even to radiation from the Cosmic Microwave Background (CMB). Based on semi-analytic models, we argue that this mechanism, occurring in the case of massive ($\geq 10^7 M_{\odot}$) molecular clouds hosting $\geq 10^6 M_{\odot}$ star clusters, allows a large mass of gas and dust to acquire a temperature below that of the CMB, whereupon dust grain growth may occur with ease. In galaxies with total stellar mass M_* , grain growth within supershells may increase the dust mass by $\sim 10^6 M_{\odot} (M_*/10^8 M_{\odot})$.

Key words: galaxies: star clusters: general — (ISM:) dust, extinction — Physical Data and Processes: hydrodynamics

1 INTRODUCTION

Violent star formation within the first $\sim 10^9$ years of cosmic time ($z \gtrsim 6$) induced a super-solar metal enrichment as observed in quasar host galaxies (e.g. Jiang et al. 2007; Calura et al. 2014). Furthermore, the detection of massive amounts of dust in the gravitationally-lensed galaxy A1750744_YD4 ($z \sim 8.38$) reveals that an early dust enrichment occurs during the epoch of cosmic reionisation (Laporte et al. 2017), when the universe was ~ 200 Myr old. It has been argued that galaxies at high-redshifts must experience a rapid (\sim a few million years long) transition between relatively dust-free and dust-rich (Mattsson et al. 2015), and that star formation may have proceeded with a top-heavy initial mass function (Gall et al. 2011; Dwek & Cherchneff 2011). Several possible dust producers at high redshift have been discussed in the literature. For example, the cold envelopes of the most massive AGB stars have been regarded as possible dust producers at high-redshift (e.g. Valiante et al. 2009; Leśniewska & Michałowski 2019), particularly in the case of a top-heavy initial mass function (Chiosi et al. 1998), while Todini & Ferrara (2001); Indebetouw et al. (2014, and references therein) have claimed that a large fraction of the early dust enrichment follows from the very fast and highly efficient dust grain condensation in supernova ejecta.

The relative importance of dust formation in supernova ejecta, dust destruction by supernova-driven shocks and dust

grain growth (by accretion of gas-phase species) in dense and cold molecular clouds (MCs) is still matter of intense debate. For instance, Calura et al. (2008, 2014), confronted the dust destruction rate obtained by McKee (1989) for SNe exploding in a three-phase interstellar medium to the dust production rates derived from galactic chemical evolutionary models (see also Dwek 1998; Zhukovska et al. 2008; Asano et al. 2013). They asserted that dust grain growth is a necessary mechanism to account for the presence of dust in galaxies, and to effectively counteract dust destruction in supernova-driven shocks. The processes of grain coagulation and grain growth are tightly related, but the former has been shown to be unimportant in calculating the evolution of the total dust mass in galaxies (Hirashita 2012). More recently, e.g. Gall & Hjorth (2018), have provided supporting evidence in that the dust content in local and high-redshift galaxies is consistent with an efficient dust production by supernovae and dust reformation shortly after destruction.

Notwithstanding, Ferrara et al. (2016) has noted that the process of grain growth must overcome several complications under the conditions prevailing in galaxies at high redshift. First, at $z \gtrsim 6$, the Cosmic Microwave Background (CMB) sets the minimum possible grain temperature as $T_{\text{cmb}} \gtrsim 20$ K (da Cunha et al. 2013), this translates into warmer grain surfaces and reduced accretion rates. Second, after the host molecular clouds are disrupted (typically in ~ 10 Myr), any material accreted onto the grain surfaces will almost immediately be photo-desorbed as the grains are exposed to the radiative feedback. A third complication arises from the

^{*} E-mail: sergiomtz@inaoep.mx

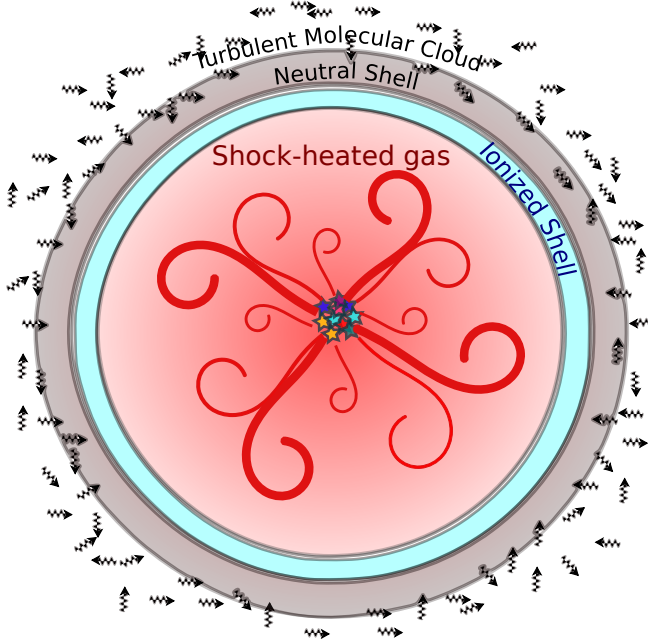


Figure 1. Schematic representation of the structure of a starburst-driven superbubble, and the central star cluster (not to scale). Each region of the superbubble is indicated: the region filled with shock-heated gas, the dense/warm ionised supershell, the very dense/cold neutral supershell, and the unshocked turbulent molecular cloud. The bath of CMB photons reaching the neutral supershell is represented by wavy arrows.

Coulomb repulsive forces between positively-charged ions and grains in the presence of a strong UV radiation field. Given the aforementioned problems, their view favours the notion that the large quantities of dust observed at high redshift must have been readily condensed in supernova ejecta. In this paper we will reexamine these objections in the context of starburst-driven superbubbles.

In the “standard bubble model”, the stellar winds of massive stars, interacting with the surrounding ISM, create a four-distinct-zone structure, namely: (i) the central hot and tenuous free wind region, (ii) a (reverse-) shocked wind region separated by a contact discontinuity from (iii) a massive, rapidly-cooling, supershell of swept-up interstellar matter that is able to absorb a large part of the impinging ionising and non-ionising radiation, and (iv) the ambient medium, an MC in our case (see [Weaver et al. 1977](#); [Mac Low & McCray 1988](#); [Koo & McKee 1992](#); [Bisnovatyi-Kogan & Silich 1995](#)). As the gas in the supershell recombines efficiently and dust absorbs large amounts of radiation, it may eventually occur that the ionisation front becomes trapped within the supershell and thus a fifth zone is formed (see Figure 1): (v) an outer dusty neutral layer in the supershell. For example, for a supershell driven by the mechanical feedback of a $10^6 M_\odot$ stellar cluster, embedded into a medium with constant density $\sim 10^3 \text{ cm}^{-3}$, the ionisation front becomes trapped in $\sim 1.5 \text{ Myr}$ ([Martínez-González et al. 2014](#)), and earlier at higher densities. Following [Weaver et al. \(1977\)](#), we will not distinguish between regions (i) and (ii), because the radius of the eventually-formed reverse shock is usually much smaller

than the radius of the forward shock. Thus, in the following we will refer to them as the shock-heated gas region.

Moreover, radiative cooling induced by dust grains ([Whitworth 2016](#)) and hydrogen-deuteride (HD) molecules, with the latter efficiently formed in post-shocked gas, may contribute to decrease the neutral supershell temperature to the floor set by the CMB ([Johnson & Bromm 2006](#)).

Furthermore, if the dust column density and the average grain cross section within the neutral supershell are sufficiently large, there is an opportunity to trap all incoming CMB radiation before reaching the supershell’s ionised part. Consequently, some part of the neutral supershell may become self-shielded from the inner starlight and from the outer CMB radiation. Interestingly, self-shielding and cooling via adiabatic expansion have been invoked to explain that the outflowing matter in the Boomerang Nebula is colder than the current CMB temperature ([Sahai & Nyman 1997](#); [Sahai et al. 2017](#)). Our investigation tests the feasibility of dust grain growth within the neutral parts of very dense ($\geq 10^6 \text{ cm}^{-3}$), dusty (with dust-to-gas mass ratio $\sim 1/150 \times Z$), and heavily pre-enriched ($\geq Z_\odot$), starburst-driven supershells.

The paper is organised as follows: Section 2 describes the superbubble model, including the equations governing the supershell’s ionised and neutral zones, and the main parameters and relevant time-scales. In Section 3 we change several parameters to explore the evolution of supershells under different ambient conditions and star cluster masses. In Section 4 we study the feasibility of dust grain growth in supershells at high-redshift. Finally, in Section 5 we summarise our conclusions.

2 THE LARGE-SCALE EVOLUTION

2.1 The Host Molecular Cloud

We consider a young massive stellar cluster located at the centre of a pre-enriched molecular cloud supported by turbulent pressure ([Elmegreen & Efremov 1997](#); [Johnson et al. 2015](#); [Calura et al. 2015](#); [Elmegreen 2017](#), see Appendix A). We assume that the molecular cloud is formed out of material with super-solar metallicity ($Z_{ISM} \geq Z_\odot$). The turbulent molecular cloud’s assumed gas density distribution is a power-law of the form (*e.g.* [Lee et al. 2015](#); [Raskutti et al. 2017](#))

$$\rho = \rho_c \left(\frac{r}{R_c} \right)^{-\omega} , \quad \text{for } r \geq R_c , \quad (1)$$

where r is the radial distance, R_c is a characteristic length scale or “core radius”, and ρ_c is the gas density at $r = R_c$. Within the central zone, we assume that the gas density distribution is homogeneous,

$$\rho = \rho_c , \quad \text{for } r < R_c . \quad (2)$$

The molecular cloud is truncated at a radius $R_{cut} \gg R_c$.

2.1.1 Superbubble Evolution

We assume that the kinetic energy injected by massive stars is thermalized in neighboring stellar wind collisions. Once the

thermalized gas pressure overcomes the turbulent pressure in the ambient molecular cloud, the shock-heated gas begins to expand. In the spherically-symmetric case, this occurs at $t_0 = 4\pi R_c^3 P_t(R_c)/(3(\gamma - 1)L_{SC})$, where L_{SC} is the star cluster mechanical luminosity, $P_t(R_c)$ is the molecular gas turbulent pressure at the star cluster edge (see Appendix A) and $\gamma = 5/3$ is the ratio of specific heats. The dynamics of the expanding bubble is determined by the set of mass, momentum and energy conservation equations (Weaver et al. 1977; Mac Low & McCray 1988; Bisnovatyi-Kogan & Silich 1995). In the case of a homogeneous ambient gas density distribution these equations have a well-known power-law solution. This solution, however, is asymptotic as it does not account for the initial conditions (at $t = 0$ years, the shell radius is zero while the shell velocity is infinite) and also it does not take into consideration the thermalized gas radiative cooling. We add to the Weaver's et al. equations the re-inserted gas radiative cooling and adopt that the ambient gas density distribution is determined by equation (1). The conservation equations that determine the starburst-driven bubble evolution then are

$$M_{sh}(r) = \frac{4\pi\rho_c R_c^3}{3-\omega} \left[\left(\frac{r}{R_c} \right)^{(3-\omega)} - 1 \right], \quad (3)$$

$$\frac{du}{dt} = \frac{4\pi r^2}{M_{sh}(r)} \left[P_b - \rho_c u^2 \left(\frac{R_c}{r} \right)^\omega \right], \quad (4)$$

$$\frac{dE_b}{dt} = L_{SC} - 4\pi r^2 P_b u - \frac{3(\dot{M}t)^2 \Lambda(T_b, Z_{ISM})}{4\pi r^3 \eta_{ion}^2}, \quad (5)$$

$$\frac{dr}{dt} = u, \quad (6)$$

where $M_{sh}(r)$ is the supershell's gas mass, the shock-heated gas thermal pressure $P_b = 3(\gamma - 1)E_b/(4\pi r^3)$, $\mu_{ion} = 14/11m_H$ is the mean mass per ion in the mass-loaded, shock-heated plasma with 1 helium atom per each 10 hydrogen atoms, m_H is the mass of the hydrogen atom, $\Lambda(T_b, Z_{ISM})$ is the Raymond et al. (1976) cooling function and $\dot{M} = 2L_{SC}/V_\infty^2$ is the mass input rate within the star cluster volume that may include the re-inserted gas mass loading by the residual gas.

The inside bubble gas mass density and temperature are

$$\rho_b = \frac{3\dot{M}t}{4\pi r^3}, \quad (7)$$

$$T_b = \frac{\mu_a P_b}{k_B \rho_b}, \quad (8)$$

where $\mu_a = 14/23m_H$ is the mean mass per particle in the completely ionised gas with 1 helium atom per each 10 hydrogen atoms and k_B is the Boltzmann constant. We solve equations (3) - (6) numerically upon the assumptions that, at $t = t_0$, the shell radius is slightly larger than the star cluster radius, $r = \alpha R_c$, the shell velocity $u = 0 \text{ km s}^{-1}$ and $\alpha = 1.05$.

In the case of a homogeneous ambient gas density distribution and negligible thermalized gas cooling, the numeric solution rapidly approaches the classic power-law solution.

If the residual gas mass is evenly incorporated into the outflow during a time t_{ml} , then the mass-loading factor is

$$\eta_{ml} = \frac{M_{MC}(r < R_c)}{\dot{M}_w t_{ml}}, \quad (9)$$

where $M_{MC}(r < R_c)$ is

$$M_{MC}(r < R_c) = \frac{4}{3}\pi\rho_c R_c^3. \quad (10)$$

As the outflow is mass-loaded, the adiabatic terminal speed is changed to

$$V_{\eta,\infty} = V_\infty(1 + \eta_{ml})^{-1/2}. \quad (11)$$

2.2 The Micro-Physics and the Shell Inner Structure

The supershell's inner structure is calculated by integrating the following set of equations, starting from the supershell's inner edge, R_b , (Draine 2011; Martínez-González et al. 2014)

$$\frac{d}{dr} \left(\frac{\mu_{ion}}{\mu_a} n k_B T \right) = n \sigma_d \frac{[L_n e^{-\tau} + L_i \phi]}{4\pi r^2 c} + \frac{n^2 \beta_2 L_i}{Q_0 c}, \quad (12)$$

$$\frac{Q_0}{4\pi r^2} \frac{d\phi}{dr} = -\beta_2 n^2 - \frac{n \sigma_d Q_0 \phi}{4\pi r^2}, \quad (13)$$

$$\frac{d\tau}{dr} = n \sigma_d. \quad (14)$$

In the above equations L_i , L_n and Q_0 are the cluster's ionising and non-ionising luminosity, and the number of ionising photons that emerge from the cluster per unit time; n and T are the supershell's gas number density and temperature, respectively; σ_d is the grain absorption cross section per particle, ϕ is the fraction of the ionising power that gets to a surface with radius r , while τ is the absorption optical depth. Finally, c and $\beta_2 = 2.59 \times 10^{-13} \text{ cm}^3 \text{ s}^{-1}$, are the speed of light, and the recombination coefficient to the excited states of H (Osterbrock 1989), respectively. The set of equations (12-14) allows to calculate the thickness of the supershell's ionised section.

The grain cross section per particle, σ_d , averaged by the Planck function, B_λ , at blackbody temperature T_λ and wavelength λ , and grain size distribution is calculated as (e.g. Ferrara et al. 2017)

$$\sigma_d = \int_{a_{min}}^{a_{max}} \int_0^\infty \frac{\pi^2 a^2 Q_{abs}(a, \lambda) B_\lambda(T_\lambda)}{\sigma_{SB} T_\lambda^4} \frac{\partial n}{\partial a} da d\lambda \quad (15)$$

where a denotes the grain radius, $Q_{abs}(a, \lambda)$ is the dust absorption efficiency (Draine 2003; Compiègne et al. 2011) and σ_{SB} is the Stefan-Boltzmann constant. σ_d in equations (12-14), is evaluated from equation (15) at the blackbody temperature of the integrated stellar spectrum (see Figure 2). At the supershell's inner edge, the boundary conditions are that τ is equal to zero and ϕ equal to unity. Given sufficient density and dust content, the ionisation front can be trapped within the supershell. This occurs when ϕ goes to zero. Thus a neutral skin is formed in the supershell's outer part (Martínez-González et al. 2014; Rahner et al. 2017), whose thickness is determined by the thermal pressure and the difference between the swept-up mass (see equation (A2)) and the mass of ionised gas.

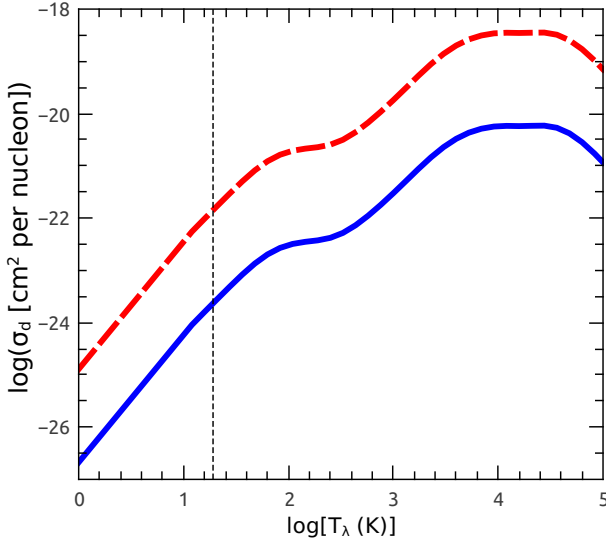


Figure 2. The grain absorption cross section per particle averaged by a log-normal grain size distribution as a function of the black-body temperature for carbonaceous grains and metallicity $2.5 Z_{\odot}$. The blue solid and red dashed lines depict σ_d for a log-normal grain size distribution (see equation 17 below) with $a_0 = 0.1 \mu\text{m}$, and $\delta = 0.01$ and $\delta = 0.05$, respectively. The vertical line indicates the value of $T_{cmb}(z = 6) = 19.1 \text{ K}$.

2.3 Neutral Shell

The optical depth to CMB photons is obtained by considering that $N_H(r')$ is the gas column density measured from the supershell's outer edge inwards:

$$\tau_{cmb}(r') = \sigma_d N_H(r') , \quad (16)$$

where σ_d is evaluated at $T_{\lambda} = T_{cmb}(z)$.

We have assumed a log-normal grain size distribution of the form (e.g. Hensley & Draine 2017)

$$\frac{\partial n}{\partial a} \sim a^{-1} \exp \left\{ -\frac{1}{2\delta^2} \left[\ln \left(\frac{a}{a_0} \right) \right]^2 \right\} , \quad (17)$$

where a_0 and δ set the peak grain size and width of the size distribution, and a_{min} and a_{max} are the lower and upper size cut-offs, respectively. The grain size distribution is normalised to the dust-to-gas mass ratio \mathcal{D} , which is assumed to scale with Z_{ISM} , as

$$\mathcal{D} = D_{\odot} Z_{ISM} = \frac{4\pi}{3\mu_{mol}} \rho_{gr} \int_{a_{min}}^{a_{max}} a^3 \frac{\partial n}{\partial a} da , \quad (18)$$

where $\mu_{mol} = 2.33 m_H$ is the mean mass of molecular gas, ρ_{gr} is the grains' bulk density (equal to 2.26 g cm^{-3} for carbonaceous grains), Z_{ISM} is measured in solar units and D_{\odot} is set to $1/150$ as in the solar vicinity.

2.3.1 Hydrogen-Deuteride Molecules (HD) and Dust Cooling

Hydrogen-deuteride molecules, efficiently formed in post-shocked gas (Vasiliev & Shchekinov 2005), allow the super-

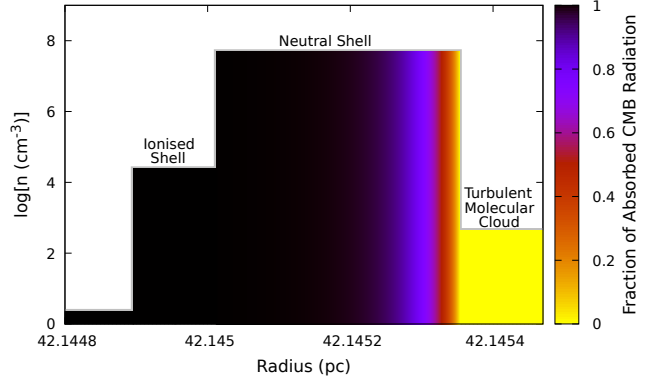


Figure 3. The supershell's gas mass density structure for model A3500 at 0.5 Myr. The supershell's ionised and neutral parts, and the cloud's unshocked part are indicated. The colour scale depicts the fraction of the CMB radiation that is trapped as it paths through the supershell.

shell's neutral part to cool down as a result of radiation emitted from their ground state rotational transition. As long as the energy levels of HD molecules are populated by CMB photons, the gas cannot cool below $T_{cmb}(z)$. The time-scale to reach the CMB temperature via HD cooling is approximated by (Johnson & Bromm 2006)

$$t_{cmb} \simeq \frac{1}{2A_{10}X_{HD}} \left(\frac{k_B T_{cmb}(z)}{h\nu_{10}} \right)^2 \exp \left(\frac{h\nu_{10}}{k_B T_{cmb}(z)} \right) , \quad (19)$$

where $A_{10} = 5 \times 10^8 \text{ s}^{-1}$ is the HD Einstein coefficient for spontaneous emission, X_{HD} is the fractional abundance of HD, $\nu_{10} \approx 2.7 \text{ THz}$ and h is the Planck constant. At $z = 6$, $t_{cmb} \approx 6.21 X_{HD}^{-1} \text{ years}$.

At densities $\gtrsim 10^6 \text{ cm}^{-3}$, however, dust grains are generally the dominant coolants (Klessen & Glover 2016) and the time required to cool the neutral supershell to $T_{cmb}(z)$ can be significantly reduced (Meece et al. 2014). The gas temperature evolution as a consequence of cooling via gas-grain collisions is given by

$$\frac{dT}{dt} = \frac{2\Lambda_{gas \rightarrow dust}}{5nk_B} , \quad (20)$$

where $\Lambda_{gas \rightarrow dust} \sim [1.2 \times 10^2 \text{ cm}^2 \text{ g}^{-1}] (\mu_{mol} n)^2 c_s^3$ (Whitworth 2016), and $c_s = (k_B T \mu_{mol}^{-1})^{1/2}$ is the isothermal sound speed. The above equation can be integrated to obtain the time required to cool the neutral supershell down to T_{cmb} . The strong radiative cooling in the supershell leads to its rapid collapse, making it extremely thin (see Figure 3).

We calculate the supershell's inner structure using time-dependent parameters, Q_0 , L_i and L_n , obtained from the Starburst99 synthesis evolutionary code (Leitherer et al. 1999). We have considered in all cases a Kroupa initial mass function sampled in the interval $(0.1 - 100) M_{\odot}$ and Padova evolutionary models including AGB stars.

3 SUPERSHELL EVOLUTION MODELS

Our reference case A3500 (see Table 1), considers a star cluster with mass $M_{SC} = 2 \times 10^6 M_{\odot}$, located within the cen-

Model	M_{SC} M_{\odot}	L_{SC} 10^{41} erg s $^{-1}$	$V_{\eta,\infty}$ km s $^{-1}$	R_c pc	R_{cut} pc	n_c cm $^{-3}$	η_{ml} —	t_{ml} Myr	M_{MC} M_{\odot}	ϵ —	ω —
A3500	2×10^6	3.12	3500	5.0	100	3.0×10^4	0.0	∞	5.3×10^7	3.7%	2.0
A1750	2×10^6	3.12	1750	5.0	100	3.0×10^4	3.0	3.8	5.3×10^7	3.7%	2.0
B3500	2×10^6	3.12	3500	5.0	48	3.0×10^4	0.0	∞	5.3×10^7	3.7%	1.5
B1750	2×10^6	3.12	1750	5.0	48	3.0×10^4	3.0	3.8	5.3×10^7	3.7%	1.5
C3500	2×10^6	3.12	3500	5.0	100	3.0×10^4	0.0	∞	2.0×10^6	10%	2.5
C1750	2×10^6	3.12	1750	5.0	100	3.0×10^4	3.0	3.8	2.0×10^6	10%	2.5
D3500	1×10^6	1.56	3500	3.0	100	5.0×10^4	0.0	∞	3.2×10^6	3.1%	2.0
D1750	1×10^6	1.56	1750	3.0	100	5.0×10^4	3.0	2.7	3.2×10^6	3.1%	2.0

Table 1. The Table presents the main parameters of our six models: the star cluster mass, the mechanical luminosity, the adiabatic terminal speed, the cloud's core and cut-off radii, the cloud's gas number density at the core radius, the mass-loading factor, the mass-loading time-scale, the molecular cloud's gas mass, the star formation efficiency, and the cloud's gas density distribution power-law index.

tral ($r < R_c = 5$ pc), dense ($n_c = \rho_c \mu_{mol}^{-1} = 3.05 \times 10^4$ cm $^{-3}$) zone of a molecular cloud (see equations 1 and 2), and a total mass $M_{MC} = 5.3 \times 10^7$ M $_{\odot}$. This assumes that the molecular cloud follows a power-law gas density distribution with $\omega = 2$ at $r \geq R_c$. This value is compatible with an isothermal, self-gravitating molecular cloud (e.g. Rahner et al. 2019, and references therein). The molecular cloud is truncated at $R_{cut} = 100$ pc and thus the star formation event occurs with a global efficiency $\epsilon \equiv M_{SC}/M_{MC} \sim 3.7\%$. The metallicity in the host molecular cloud is chosen as 2.5 Z $_{\odot}$. This choice is motivated by the rapid build-up of metals in starbursting quasar-host galaxies where the gas metallicity reaches super-solar values already at ~ 0.1 Gyr (e.g. Calura et al. 2014). According to the outputs from Starburst99, the values of L_{SC} and V_{∞} at the start of the cluster's evolution are $\sim 3.12 \times 10^{41}$ erg s $^{-1}$ and ~ 3500 km s $^{-1}$, respectively, implying a star cluster's mass loss rate of $\dot{M}_w \sim 8.0 \times 10^{-2}$ M $_{\odot}$ yr $^{-1}$.

The fractional HD abundance is selected as $X_{HD} = 6.8 \times 10^{-5}$ (Meece et al. 2014). This implies, from evaluation of equation (19), that the neutral supershell reaches the CMB temperature in $\sim 9.13 \times 10^4$ years via HD cooling alone. However, if one accounts for dust cooling (equation 20), the time required to reach $T_{cmb} = 19.1$ K would be ~ 350 years if the supershell's neutral section has an initial temperature $\sim 10^4$ K (right after it ceases to be ionised) and a density $\sim 9.4 \times 10^5$ cm $^{-3}$. Moreover, dust-induced cooling is largely capable of counteracting the heating induced by H $_2$ formation at densities $\geq 10^6$ cm $^{-3}$ and metallicities $\geq 10^{-2}$ Z $_{\odot}$ (Meece et al. 2014).

Regarding the grain size distribution defined in equation (17), we have fixed $\delta = 0.05$, $a_0 = 0.1$ μm , $a_{min} = 0.001$ μm and $a_{max} = 0.5$ μm . For simplicity we consider only carbonaceous grains. We have imposed that supershells effectively self-shield from the CMB only when $[1 - \exp(-\tau_{cmb})] \geq 99.0\%$. For the sake of comparison, seven additional cases (A1750, B3500, B1750, C3500, C1750, D3500 and D1750) were also considered. The chosen parameters in all of them fall within the observational constraints derived for the case of a molecular cloud ($\sim 9 \times 10^7$ M $_{\odot}$) at $z \sim 6$, hosting a compact protoglobular cluster candidate with a stellar mass of a few $\sim 10^6$ M $_{\odot}$ (Vanzella et al. 2019; Calura et al. 2021).

Model A1750 ($\epsilon \sim 3.7\%$) differs from the reference case A3500 as it includes mass-loading that results in a terminal speed $V_{\eta} = 1750$ km s $^{-1}$. Models B3500 and B1750 ($\epsilon \sim 3.7\%$) as-

sume a flatter gas density distribution ($\omega = 1.5$). This choice is supported by the results of Lee et al. (2015) and Raskutti et al. (2017). Models C3500 and C1750 ($\epsilon \sim 10.0\%$) consider a steeper gas density distribution ($\omega = 2.5$). Finally, models D3500 and D1750 ($\epsilon \sim 3.1\%$) explore the case of a central star cluster with 10 6 M $_{\odot}$. All models denoted with 3500 have $V_{\eta} = 3500$ km s $^{-1}$. Models with 1750 correspond to mass-loaded outflows with $V_{\eta} = 1750$ km s $^{-1}$, $\eta_{ml} = 3.0$, and $t_{ml} = 3.8$ Myr for models A1750, B1750 and C1750, and $t_{ml} = 2.7$ Myr for model D1750. The central zone gas mass is $M_{MC}(r < R_c) \sim 9.2 \times 10^5$ M $_{\odot}$ in all but models D3500 and D1750. In those models, $M_{MC}(r < R_c) \sim 3.3 \times 10^5$ M $_{\odot}$. In models A3500, A1750, C3500, C1750, D3500 and D1750, we have truncated the clouds at $R_{cut} = 100$ pc. For models B3500 and B1750 the clouds are truncated at $R_{cut} = 48$ pc so they have the same mass than in the reference case. In all models we have selected a redshift $z = 6$. Our calculations are stopped once the supershells reach the edge of their host molecular cloud. The input parameters are summarised in Table 1. In all the presented cases, the outward-directed force resulting from the shock-heated gas thermal pressure overcomes the inward-directed gravitational force acting on the supershell during the whole supershell evolution:

$$P_b > \frac{1}{4\pi r^2} \left(\frac{GM_{sh}(r)M_0}{r^2} + \frac{1}{2} \frac{GM_{sh}^2}{r^2} \right), \quad (21)$$

where $M_0 = M_{MC}(r < R_c) + M_{SC}$. This warrants that the star cluster's mechanical energy is sufficient to overcome the binding energy of the star cluster (Baumgardt et al. 2008) and form an expanding supershell.

In our reference model A3500, the supershell self-shields from the star cluster ionising and non-ionising radiation as soon as it starts to grow (*i.e.* both $(1 - \phi)$ and $[1 - \exp(-\tau)]$ go rapidly to unity).

Figure 3 presents the density structure of the starburst-driven supershell at 0.5 Myr of evolutionary time in the reference model A3500. In this case, the fraction of CMB radiation that is absorbed within the supershell's neutral part is remarkably high, with $[1 - \exp(-\tau_{cmb})]$ reaching $\gtrsim 99.9\%$, during ~ 0.65 Myr, and $\gtrsim 99.0\%$ during ~ 1.0 Myr. In all models with mass-loading (decreased terminal speed), the supershell self-shields from the CMB radiation for a longer time. Interestingly, if we consider a flatter gas density distribution, as in cases B3500 and B1750, the self-shielded gas mass in-

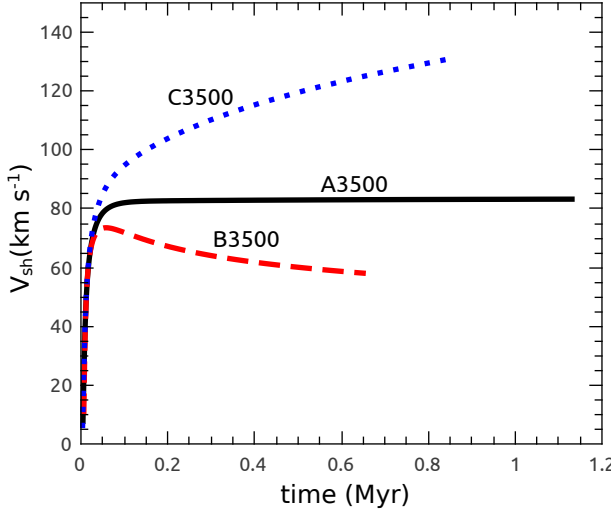


Figure 4. The supershell expansion velocity in different molecular gas density distributions for models A3500 (black solid line), B3500 (red dashed line), and C3500 (blue dotted line). Note that the calculations are stopped when the supershells reach the edge of their host molecular clouds.

crements monotonically, and the supershells in those cases maintain $[1 - \exp(-\tau_{cmb})] \gtrsim 99.9\%$ during the whole time they evolve within their host molecular cloud (see Section 4). Models C3500, C1750, D3500 and D1750 show similar trends to the ones observed in models A3500 and A1750, but the time in which $[1 - \exp(-\tau_{cmb})] \gtrsim 99\%$ is reduced to ~ 0.36 Myr, ~ 0.4 Myr, ~ 0.6 Myr, and ~ 0.75 Myr, respectively. The supershell expansion velocity in different ambient gas density distributions is shown in Figure 4, where solid, dashed and dotted lines correspond to models A3500, B3500 and C3500, respectively. The supershells in all our models do not stall within their host molecular clouds. However, in clouds with a power-law index $\omega > 2$, the supershells accelerate and, inevitably, become Rayleigh-Taylor unstable (Krause et al. 2012). Note also that in simulations with larger mass-loading rates (terminal speeds $V_\eta < 1500$ km s⁻¹), catastrophic gas cooling sets in the shock-heated gas zone that prevents the formation of supershells.

We have restricted our models to the spherically-symmetric case. However, if the host molecular cloud is clumpy, the starburst-driven superbubble would expand preferentially through channels in between clumps (Lucas et al. 2020). We will explore that scenario in a forthcoming communication by means of three-dimensional hydrodynamical simulations.

4 THE GROWTH OF DUST GRAINS

As a consequence of the supershell's self-shielding against the incoming CMB/starlight radiation, the restrictions for dust grain growth at high-redshift (Ferrara et al. 2016) are evaded. Indeed in this case:

- Dust grains in supershells can cool below T_{cmb} . For instance, a dust grain would take just a few days to cool down to 15 K or less (see Appendix B).

- The grains will not photo-desorb their accreted species, nor will they become Coulomb repulsive.

The grain growth time-scale is given by (Spitzer 1978)

$$t_{growth} = \left[\frac{3SD\mu_{mol}n}{4\rho_{gra}} \left(\frac{8k_B T}{\pi m_s} \right)^{1/2} \right]^{-1}, \quad (22)$$

where $S = [0, 1]$ is the sticking coefficient, and m_s is the mass of the accreting species. The redshift-dependent CMB photon number density is given by (e.g. Grupen 2005)

$$n_\gamma = 16\pi\zeta(3) \left(\frac{kT_{CMB}(z)}{ch} \right)^3, \quad (23)$$

where ζ is the Riemann zeta function. The CMB photon number density scales with redshift as $\approx 411(1+z)^3$ cm⁻³, so its value (attenuated by dust absorptions) at $z = 6$ is $\approx 1.41 \times 10^5 [1 - \exp(-\tau_{cmb}(r'))]$ cm⁻³. The dust absorption rate per unit volume for the case of CMB photons, is

$$\kappa_{cmb} = n\sigma_d F_\gamma [1 - \exp(-\tau_{cmb}(r'))], \quad (24)$$

where $F_\gamma = n_\gamma \times c/\sqrt{3}$ is the mean CMB photon flux (Heacox 2017; Kim et al. 2019).

Figure 5, panel a, shows κ_{cmb} calculated at the inner edge of the neutral supershell. In all cases κ_{cmb} is tiny during much of the supershell's evolution. This implies that the CMB radiation and the gas and dust are thermally-decoupled. Panel b in the same Figure shows that, initially, the self-shielded gas mass increases as it collects more mass. However, depending on the cloud's radial gas density distribution, the fast supershell expansion eventually leads to a decreased supershell's density. This provokes a decline in the amount of self-shielded gas mass in the case of a steep ambient gas density distribution (in cases A3500 and A1750 this occurs after ~ 0.5 Myr). This decline does not occur for our models with a flatter ($\rho \sim r^{1.5}$) gas density distribution.

The grain growth time-scale within the neutral supershell is so fast in our models (see panel c in Figure 5) and the dust-induced cooling is so efficient, that one can expect that all the available refractory elements will inevitably be accreted onto dust grains. For instance, for $a = 0.01$ μm , $S = 1$, and $T = T_{cmb}(z = 6)$, t_{growth} is $\lesssim 100$ years during the first ~ 2 Myr, while if S acquires a modest value, e.g. 0.1, t_{growth} would be $\lesssim 1000$ years during that period. Panel c also shows that adiabatic cooling (lines above the axis break, see equation B3 in Appendix B) is at play, but with a reduced effect due to its significantly longer characteristic time-scale. Hence, grains can grow very rapidly in the extremely dense, heavily-enriched and cold neutral part of the dusty supershell. For an assumed maximum dust-to-gas mass ratio $\sim 1/100$ (Valentini & Brighenti 2015) at solar metallicity, scaling with Z_{ISM} , the dust mass will have a net increase of $\sim 8.8 \times 10^4$ M_⊙ for model A3500, and $\sim 8.6 \times 10^4$ M_⊙ for model A1750. In models B3500 and B1750, the dust mass increase is $\sim 3.26 \times 10^5$ M_⊙ and $\sim 3.31 \times 10^5$ M_⊙, respectively. The accelerating supershells in models C3500 and C1750 rupture as they become Rayleigh-Taylor unstable, and consequently, it is uncertain whether dust grain growth could occur. Nevertheless, we report the results of our calculations for these models in Figure 6. Finally, the dust mass increments are

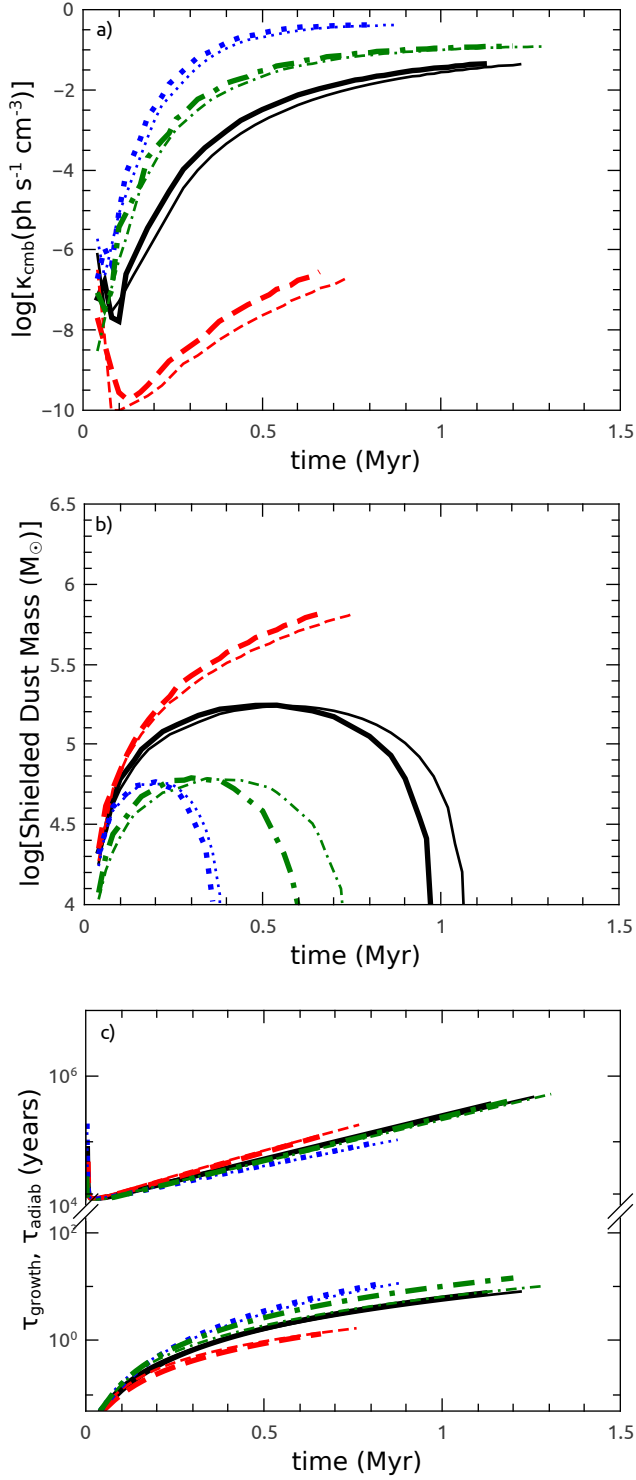


Figure 5. The starburst-driven supershell properties. Panel a presents the dust absorption rate per unit volume. The amount of dust in the self-shielded region as a function of time is presented in panel b. Lines below and above the axis break on panel c display the adiabatic cooling and the dust grain growth (for $S = 1$ and $a = 0.01 \mu\text{m}$) time-scales, respectively. In each panel, we present the results for the A3500 (thick black solid lines), A1750 (thin black solid lines), B3500 (thick red dashed lines), B1750 (thin red dashed lines), C3500 (thick blue dotted lines), C1750 (thin blue dotted lines), D3500 (thick dash-dotted lines) and D1750 (thin dash-dotted lines) cases, respectively.

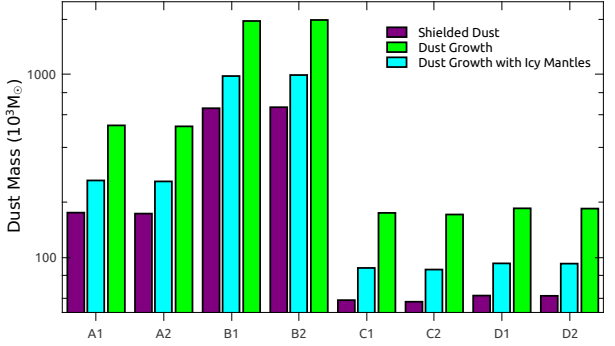


Figure 6. Bar graph of the growth of dust mass in the self-shielded region for each studied case. The bars in purple, cyan and green indicate the pre-existent swept-up dust mass in the self-shielded region (in units $10^3 M_\odot$), the growth of the dust mass due to accretion of refractory elements, and the estimated growth of dust mass due to icy mantles, respectively.

$\sim 3.1 \times 10^4 M_\odot$ for both models D3500 and D1750. The above quantities disregard the dust mass in the form of ice mantles, which can further boost the grains' mass. The bars in Figure 6 represent the amount of dust that was originally swept-up (purple), the amount of dust that is obtained after all refractory elements are locked-up onto the grains (cyan), and the grain mass in the form of ice mantles, which is assumed to increase the total dust mass by a factor of two (Kruegel 2003). As a result, the supershells' self-shielded sections will have, within ~ 1 Myr, three times more dust mass than the original self-shielded dust mass.

As expected, the most successful cases are those in which the stellar masses are larger. If one assumes a cluster mass function $dN/dM_* \propto M_*^\beta$, with $\beta \approx -2$ (e.g. Cook et al. 2019), in a galaxy with lower and upper cluster masses $10^3 M_\odot$ and $10^7 M_\odot$, respectively, then the number of clusters with masses $\gtrsim 10^6 M_\odot$ scales as $\sim 10(M_*/10^8 M_\odot)$. In the above M_* stands for the total stellar mass. If the typical net increment in dust mass within CMB-dark supershells in clusters with $\gtrsim 10^6 M_\odot$ is $\sim 10^5 M_\odot$ (and all of them reside within dense molecular clouds), then the proposed mechanism can account for the build-up of $\sim 10^6 M_\odot (M_*/10^8 M_\odot)$ of dust.

This rough estimate takes into account that the fraction of stars that form in bound clusters grows with redshift, and at $z \sim 6$ they likely made the larger proportion (e. g. Vanzella et al. 2019, and references therein).

We have seen so far that dust grain growth within starburst-driven supershells can be both very rapid and very efficient in time-scales of order $\lesssim 1$ Myr, before any supernova goes off in the central starburst. However, between $\sim 3 - 40$ Myr, the massive stars in the clusters will explode as core-collapse supernovae. In that scenario, supernova blast waves will ram through the hot gas cavity and collide with the encompassing supershell. Such situation was studied by Martínez-González et al. (2018, 2019) by means of three-dimensional hydrodynamical simulations. Upon the collision, the supernova remnants become strongly radiative and do not experience the Sedov-Taylor phase (see Figure 5 in Martínez-González et al. 2019). Moreover, blast waves are mostly reflected and soon catch up with the reverse shock as they only penetrate a very thin layer into the supershell (Tenorio-Tagle et al. 1990).

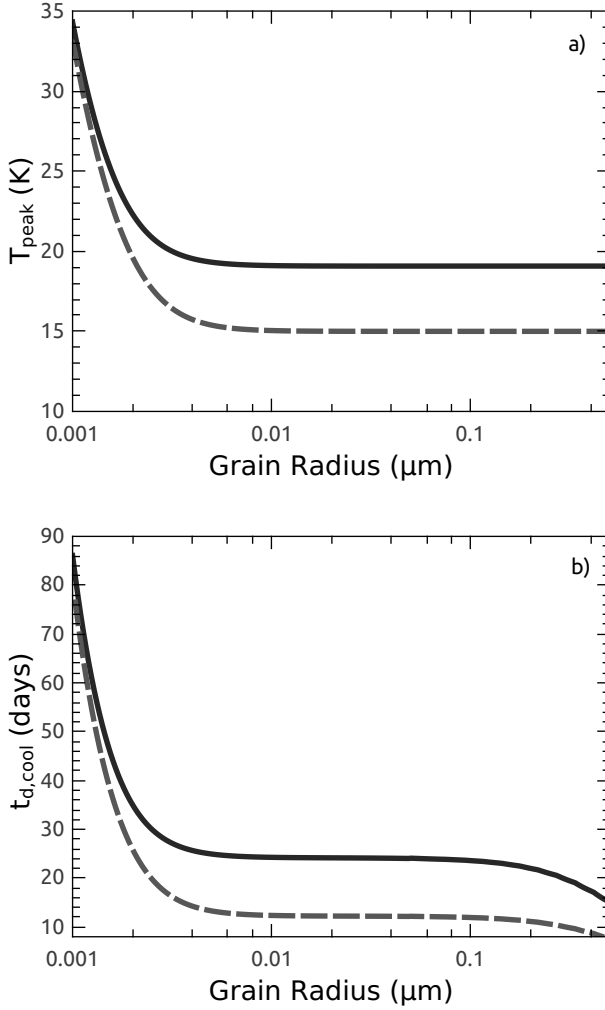


Figure 7. T_{peak} as a function of grain radius for the case of grains colliding with an HD-emitted photon (panel a). The time required to cool from T_{peak} to $T_d = 10$ K as a function of grain radius (panel b). In both panels the solid lines assume the initial grain temperature to be 19.1 K, while the dashed lines depict the case for an initial grain temperature equal to 15 K.

Thus, the dust grains locked-up in the supershell will remain largely unaffected.

Supershells may eventually become pressure-confined, perhaps outside their host molecular clouds, and the time required for them to stall is shorter than the life-time of massive stars and their continuous winds (several tens of Myr). This implies that the central cluster will continue to produce a high velocity outflow ($\gtrsim 1000$ km s $^{-1}$). The dense ($\gtrsim 10^6$ cm $^{-3}$) stalling supershell rests then above a lower density ($\lesssim 10^{-1}$ cm $^{-3}$), hot ($\gtrsim 10^7$ K) gas. In that case the standing supershell feels an inward gravity and becomes Rayleigh-Taylor unstable. Consequently, the blast waves will collide with supershell fragments and the hot ejecta will pass through channels in between them, establishing pressure equilibrium. The blast waves will then attempt to ram through the fragments, but one can expect that they will only be weakly transmitted.

Thus the large majority of the supershell's dust grains will survive to eventually mix with the unshocked ISM.

This situation differs from that described by Weaver et al. (1977) (our models with $\omega \leq 2.0$), where decelerating supershells are stable because the hot gas rests on top of the dense expanding supershell, and then a co-moving parcel of fluid feels an effective *outward* gravity.

5 CONCLUDING REMARKS

Based on semi-analytic models, we have analysed the large-scale evolution of starburst-driven supershells and the micro-physics of the dust grain growth process within supershells at high-redshift ($z \sim 6$).

The main model predictions are summarised as follows:

- Supershells can self-shield from the stellar radiation field and from the Cosmic Microwave Background. The latter requires them to be sufficiently metal-rich ($Z \geq Z_\odot$), dense ($n \geq 10^6$ cm $^{-3}$) and dusty ($\mathcal{D} \sim 1/150 \times Z$), and that the gas density distribution in the host molecular cloud is not too steep ($\omega \leq 2$).
- As a result of dust-induced and HD cooling (and less importantly adiabatic expansion), the supershell's dust grains can cool below the temperature set by the CMB ($T_{cmb}(z = 6) = 19.1$ K), *e.g.* to a temperature ~ 15 K or less within a few days.
- The grain growth time-scale in the self-shielded section of supershells is sufficiently short ($\lesssim 100$ years) to allow all refractory elements within the supershell's self-shielded section to be accreted onto dust grains.
- These grains do not photo-adsorb the accreted species, nor become Coulomb repulsive, and thus can survive being self-shielded from the central cluster starlight.
- The total amount of dust produced by this mechanism may reach $\sim 10^6 M_\odot (M_*/10^8 M_\odot)$.

This mechanism takes place before the first supernova explosion in the central star cluster (~ 3 Myr). Nevertheless, supernovae do not pose a significant threat to the survival of the dust grains locked-up within the encompassing supershell because the latter mostly reflects the colliding blast waves, leaving its dust content largely unaffected (Martínez-González et al. 2019). We have thus shown that dust grain growth at high redshift may take place rapidly and efficiently.

6 ACKNOWLEDGEMENTS

This study was supported by CONACYT-México research grant A1-S-28458. S.M.G. also acknowledges support by CONACYT through Cátedra n.482. The authors thankfully acknowledge the computer resources, technical expertise and support provided by the Laboratorio Nacional de Supercómputo del Sureste de México, CONACYT member of the network of national laboratories, and by the Laboratorio Nacional de Cómputo de Alto Desempeño (LANCAD), project 13-2021. The authors thank the anonymous Referee for a careful reading and helpful suggestions which greatly improved the paper.

7 DATA AVAILABILITY

The data underlying this article will be shared on reasonable request to the corresponding author.

REFERENCES

Asano R. S., Takeuchi T. T., Hirashita H., Nozawa T., 2013, *MNRAS*, **432**, 637

Badjin D. A., Glazyrin S. I., Manukovskiy K. V., Blinnikov S. I., 2016, *MNRAS*, **459**, 2188

Baumgardt H., Kroupa P., Parmentier G., 2008, *MNRAS*, **384**, 1231

Bisnovatyi-Kogan G. S., Silich S. A., 1995, *Reviews of Modern Physics*, **67**, 661

Calura F., Pipino A., Matteucci F., 2008, *A&A*, **479**, 669

Calura F., Gilli R., Vignali C., Pozzi F., Pipino A., Matteucci F., 2014, *MNRAS*, **438**, 2765

Calura F., Few C. G., Romano D., D'Ercole A., 2015, *ApJ Let*, **814**, L14

Calura F., et al., 2021, *MNRAS*, **500**, 3083

Chiosi C., Bressan A., Portinari L., Tantalo R., 1998, *A&A*, **339**, 355

Compiègne M., et al., 2011, *A&A*, **525**, A103

Cook D. O., et al., 2019, *MNRAS*, **484**, 4897

Draine B. T., 2003, *ApJ*, **598**, 1026

Draine B. T., 2011, *ApJ*, **732**, 100

Dwek E., 1986, *ApJ*, **302**, 363

Dwek E., 1998, *ApJ*, **501**, 643

Dwek E., Cherchneff I., 2011, *ApJ*, **727**, 63

Elmegreen B. G., 2017, *ApJ*, **836**, 80

Elmegreen B. G., Efremov Y. N., 1997, *ApJ*, **480**, 235

Ferrara A., Viti S., Ceccarelli C., 2016, *MNRAS*, **463**, L112

Ferrara A., Hirashita H., Ouchi M., Fujimoto S., 2017, *MNRAS*, **471**, 5018

Gall C., Hjorth J., 2018, *ApJ*, **868**, 62

Gall C., Hjorth J., Andersen A. C., 2011, *A&ARv*, **19**, 43

Grupen C., 2005, *Astroparticle Physics*, doi:10.1007/s-3-540-27670-X

Heacox W. D., 2017, *Contemporary Physics*, **58**, 190

Hensley B. S., Draine B. T., 2017, *ApJ*, **836**, 179

Hirashita H., 2012, *MNRAS*, **422**, 1263

Indebetouw R., et al., 2014, *ApJ Let*, **782**, L2

Jiang L., Fan X., Vestergaard M., Kurk J. D., Walter F., Kelly B. C., Strauss M. A., 2007, *AJ*, **134**, 1150

Johnson J. L., Bromm V., 2006, *MNRAS*, **366**, 247

Johnson K. E., Leroy A. K., Indebetouw R., Brogan C. L., Whitmore B. C., Hibbard J., Sheth K., Evans A. S., 2015, *ApJ*, **806**, 35

Kim J.-G., Kim W.-T., Ostriker E. C., 2019, *ApJ*, **883**, 102

Klessen R. S., Glover S. C. O., 2016, *Saas-Fee Advanced Course*, **43**, 85

Koo B.-C., McKee C. F., 1992, *ApJ*, **388**, 93

Krause M., Charbonnel C., Decressin T., Meynet G., Prantzos N., Diehl R., 2012, *A&A*, **546**, L5

Kruegel E., 2003, The physics of interstellar dust

Laporte N., et al., 2017, *ApJ Let*, **837**, L21

Lee E. J., Chang P., Murray N., 2015, *ApJ*, **800**, 49

Leitherer C., et al., 1999, *ApJ*, **123**, 3

Leśniewska A., Michałowski M. J., 2019, *A&A*, **624**, L13

Lucas W. E., Bonnell I. A., Dale J. E., 2020, *MNRAS*, **493**, 4700

Mac Low M.-M., McCray R., 1988, *ApJ*, **324**, 776

Martínez-González S., Silich S., Tenorio-Tagle G., 2014, *ApJ*, **785**, 164

Martínez-González S., Tenorio-Tagle G., Silich S., 2016, *ApJ*, **816**, 39

Martínez-González S., Wünsch R., Palouš J., 2017, *ApJ*, **843**, 95

Martínez-González S., Wünsch R., Palouš J., Muñoz-Tuñón C., Silich S., Tenorio-Tagle G., 2018, *ApJ*, **866**, 40

Martínez-González S., Wünsch R., Silich S., Tenorio-Tagle G., Palouš J., Ferrara A., 2019, *ApJ*, **887**, 198

Mattsson L., Gomez H. L., Andersen A. C., Matsuura M., 2015, *MNRAS*, **449**, 4079

McKee C., 1989, in Allamandola L. J., Tielens A. G. G. M., eds, Vol. 135, *Interstellar Dust*. p. 431

Meece G. R., Smith B. D., O'Shea B. W., 2014, *ApJ*, **783**, 75

Osterbrock D. E., 1989, *Astrophysics of gaseous nebulae and active galactic nuclei*. Mill Valley, CA: University Science Books

Rahner D., Pellegrini E. W., Glover S. C. O., Klessen R. S., 2017, *MNRAS*, **470**, 4453

Rahner D., Pellegrini E. W., Glover S. C. O., Klessen R. S., 2019, *MNRAS*, **483**, 2547

Raskutti S., Ostriker E. C., Skinner M. A., 2017, *ApJ*, **850**, 112

Raymond J. C., Cox D. P., Smith B. W., 1976, *ApJ*, **204**, 290

Sahai R., Nyman L.-Å., 1997, *ApJ Let*, **487**, L155

Sahai R., Vlemmings W. H. T., Nyman L. Å., 2017, *ApJ*, **841**, 110

Spitzer L., 1978, *Physical processes in the interstellar medium*, doi:10.1002/9783527617722

Tenorio-Tagle G., Bodenheimer P., Franco J., Rozyczka M., 1990, *MNRAS*, **244**, 563

Todini P., Ferrara A., 2001, *MNRAS*, **325**, 726

Valentini M., Brightenti F., 2015, *MNRAS*, **448**, 1979

Valiante R., Schneider R., Bianchi S., Andersen A. C., 2009, *MNRAS*, **397**, 1661

Vanzella E., et al., 2019, *MNRAS*, **483**, 3618

Vasiliev E. O., Shchekinov Y. A., 2005, *Astrophysics*, **48**, 491

Weaver R., McCray R., Castor J., Shapiro P., Moore R., 1977, *ApJ*, **218**, 377

Whitworth A. P., 2016, *MNRAS*, **458**, 1815

Zhukovska S., Gail H. P., Trieloff M., 2008, *A&A*, **479**, 453

da Cunha E., et al., 2013, *ApJ*, **766**, 13

APPENDIX A: TURBULENT MOLECULAR CLOUD

The pressure gradient in the static initial cloud is determined by the equation (e.g. Calura et al. 2015)

$$\frac{dP_t}{dr} = \frac{-GM(r)\rho}{r^2}, \quad (\text{A1})$$

where G is the gravitational constant. In the case of a power-law density distribution (see equation 1), the mass enclosed within a radius r , $M_{MC}(r)$, is

$$M_{MC}(r) = M_0 + \frac{4\pi\rho_c R_c^3}{(3-\omega)} \left[\left(\frac{r}{R_c} \right)^{3-\omega} - 1 \right], \quad (\text{A2})$$

where M_0 is the total (the star cluster and the residual gas) mass within the central zone with radius $r < R_c$. The second term in equation (A2) gives the mass contained in the swept-up supershell, M_{sh} .

In the case of a power-law density distribution, equation (A1) is easily integrated:

$$P_t = \frac{GM_0\rho_c}{(\omega+1)R_c} \left(\frac{r}{R_c} \right)^{-(\omega+1)} + \frac{2\pi G\rho_c^2 R_c^2}{(3-\omega)(\omega-1)} \times \left[\left(\frac{r}{R_c} \right)^{2(1-\omega)} - \frac{2(\omega-1)}{\omega+1} \left(\frac{r}{R_c} \right)^{-(\omega+1)} \right], \quad (\text{A3})$$

if $\omega > 1$ and $P_t(\infty) = 0$.

APPENDIX B: HEATING AND COOLING IN THE SELF-SHIELDED NEUTRAL SHELL

Dust grains residing within the supershell's self-shielded, neutral part do not experience stochastic temperature fluctuations due to collisions with CMB photons, however, they still have temperature fluctuations as they collide with neutral species and/or absorb HD-emitted ($h\nu_{10} \sim 1.1 \times 10^{-2}$ eV) and infrared re-emitted photons. After each collision/absorption event, a dust grain with initial temperature T_0 will be heated to a peak temperature, T_{peak} , given by

$$E = \int_{T_0}^{T_{peak}} C(a, T_d) \, dT_d. \quad (\text{B1})$$

where $C(a, T_d)$ is the grain heat capacity as a function of the grain's radius, chemical composition and temperature, T_d . Upon reaching T_{peak} , the grain starts to cool down in a time-scale given by (Dwek 1986; Martínez-González et al. 2016, 2017)

$$t_{d,cool} = \int_{T_d}^{T_{peak}} \frac{C(a, T_d) \, dT_d}{|4\pi a^2 \sigma_{SB} \langle Q_{abs} \rangle T_d^4|}, \quad (\text{B2})$$

where $\langle Q_{abs} \rangle$ is the Planck-averaged grain absorption efficiency. Figure 7 shows T_{peak} and $t_{d,cool}$ as a function of grain radius for the case of grains colliding with an HD-emitted photon, whose energy roughly corresponds with the energy of an infrared photon with wavelength ~ 100 μm . We have assumed values of T_0 equal to 15 K and 19.1 K. A significant temperature increase will be expected only for grains $a \leq 0.003$ μm , while $t_{d,cool}$ between T_{peak} and $T_d = 10$ K takes only some tens of days.

On the other hand, the supershell cools as it expands and the characteristic time-scale for adiabatic cooling is (Badjin et al. 2016)

$$t_{adiab} = \frac{(\gamma + 1)}{6(\gamma - 1)} \frac{R_S}{V_S}, \quad (\text{B3})$$

where R_S and V_S are the forward shock radius and velocity.

This paper has been typeset from a $\text{TeX}/\text{L}\text{A}\text{T}\text{E}\text{X}$ file prepared by the author.